Geochemistry Geophysics Geosystems G3
AN ELECTRONIC JOURNAL OF THE EARTH SCIENCES
Published by AGU and the Geochemical Society

*Article*
Volume 6, Number 11
29 November 2005
Q11012, doi:10.1029/2005GC000998
ISSN: 1525-2027

# Numerical evidence for thermohaline circulation reversals during the Maastrichtian

**Emmanuelle Pucéat**
*Laboratoire des Sciences du Climat et de l'Environnement (LSCE), UMR CEA/CNRS 1572, CE Saclay, Orme des Merisiers, Bat. 701, F-91191 Gif sur Yvette Cedex, France*

*Géosciences Rennes UMR CNRS 6118, Block 15, Université de Rennes1, Campus de Beaulieu, CS 74205, F-35042 Rennes Cedex, France*

*Now at Université de Bourgogne, Laboratoire Biogéosciences, UMR CNRS 5561, 6 Bd. Gabriel, F-21000 Dijon, France (emmanuelle.puceat@u-bourgogne.fr)*

**Yannick Donnadieu and Gilles Ramstein**
*Laboratoire des Sciences du Climat et de l'Environnement (LSCE), UMR CEA/CNRS 1572, CE Saclay, Orme des Merisiers, Bat. 701, F-91191 Gif sur Yvette Cedex, France*

**Frédéric Fluteau**
*Institut de Physique du Globe de Paris, T24-25 E1, 4 Place Jussieu, F-75252 Paris Cedex 05, France*

**François Guillocheau**
*Géosciences Rennes UMR CNRS 6118, Block 15, Université de Rennes1, Campus de Beaulieu, CS 74205, F-35042 Rennes Cedex, France*

[1] The sensitivity of the Maastrichtian thermohaline circulation to the opening/closing of marine communications between the Arctic and North Pacific oceans is investigated through a set of numerical experiments using the model CLIMBER-2 (Earth Model of Intermediate Complexity). We show here that the opening or closing of an Arctic-Pacific marine gateway induces transitions between different equilibrium states of the thermohaline circulation. Sensitivity tests of the inferred modes of thermohaline circulation to atmospheric $CO_2$ level changes have also been explored. An abrupt switch in deep convection from high northern to high southern latitudes, a change consistent with isotopic evidences, is reproduced by our simulations. The switch is caused by a combination of increased atmospheric $CO_2$ concentration and inflow in the North Pacific of low-salinity Arctic waters when the Arctic-Pacific marine gateway is opened. The state of the gateway (open/closed) may have changed rapidly through variations in sea level that have been inferred for the Maastrichtian period.

**Components:** 6971 words, 9 figures.

**Keywords:** climate model; Cretaceous; Maastrichtian; thermohaline circulation.

**Index Terms:** 1626 Global Change: Global climate models (3337, 4928); 4901 Paleoceanography: Abrupt/rapid climate change (1605); 4962 Paleoceanography: Thermohaline.

**Received** 12 April 2005; **Revised** 29 August 2005; **Accepted** 30 September 2005; **Published** 29 November 2005.

Pucéat, E., Y. Donnadieu, G. Ramstein, F. Fluteau, and F. Guillocheau (2005), Numerical evidence for thermohaline circulation reversals during the Maastrichtian, *Geochem. Geophys. Geosyst.*, *6*, Q11012, doi:10.1029/2005GC000998.

## 1. Introduction

[2] The latest part of the Cretaceous period (Maastrichtian) has been inferred to be a time of high variability in the climate/ocean system [*Barrera*, 1994; *MacLeod and Huber*, 1996; *Li and Keller*, 1998]. Fluctuations in $\delta^{18}O$ and $\delta^{13}C$ values of planktonic and benthic foraminifera from different areas of the Pacific, Atlantic, and Indian oceans suggest the existence of different modes of thermohaline circulation within the Maastrichtian interval [*Barrera et al.*, 1997; *Barrera and Savin*, 1999; *Frank and Arthur*, 1999]. More specifically, the mid-Maastrichtian period is thought to have witnessed a reversal in the thermohaline circulation pattern, from an oceanic circulation driven by deep water formation in the North Pacific in the Early Maastrichtian, to deep water formation in the Southern Ocean during the Late Maastrichtian, in a mode more similar to today's [*Barrera and Savin*, 1999; *Frank and Arthur*, 1999]. The northern North Atlantic Ocean has also been proposed as a site for intermediate or deep water production during the Maastrichtian [*Frank and Arthur*, 1999]. Spreading of this water mass outside of the North Atlantic would, however, have been precluded before the mid-Maastrichtian by the existence of tectonic structures on the South Atlantic Ocean floor like the Rio Grande Rise-Walvis Ridge system [*Frank and Arthur*, 1999].

[3] The driving mechanisms of the reversal in thermohaline circulation patterns during the mid-Maastrichtian suggested by isotopic data are still debated [*Barrera and Savin*, 1999; *Frank and Arthur*, 1999]. Climate models can be used to explore the driving mechanisms of climate and oceanic circulation changes. However, most of the previous simulations using General Circulation Models (GCM) for the Cretaceous period were conducted for the mid Cretaceous [e.g., *Barron et al.*, 1995; *Poulsen et al.*, 1999, 2003] and simulations exploring the latest Cretaceous period (Campanian-Maastrichtian) still remain quite limited and contradictory [*Bush and Philander*, 1997; *Brady et al.*, 1998; *DeConto et al.*, 2000; *Otto-Bliesner et al.*, 2002]. More specifically, the previously published latest Cretaceous simulations show either a presence [*Otto-Bliesner et al.*, 2002] or an absence [*Brady et al.*, 1998; *DeConto et al.*, 2000] of deep water formation in the North Pacific. In addition, as it takes a long time to run 3-D GCM until equilibrium conditions, no simulations have ever been done over the large range of atmospheric $CO_2$ levels inferred from latest Cretaceous proxy records [*Royer et al.*, 2004] or slightly different paleogeography to test the impact of these factors on Maastrichtian climate and oceanic circulation. Such simulations are, however, essential to explore Maastrichtian changes in thermohaline circulation, since the reversal in thermohaline circulation has been tentatively linked to changes in climate and sea level [*Barrera et al.*, 1997].

[4] In order to overcome the high computational cost of AOGCMs, the Earth system Model of Intermediate Complexity (EMIC) CLIMBER-2 is used in this study. The ocean-atmosphere coupled model, CLIMBER-2, describes a large set of processes and feedbacks, but due to low spatial resolution and simplified governing equations, has a fast turnaround time. Mechanisms of oceanic circulation changes within the Maastrichtian period are carefully examined through a suite of sensitivity experiments testing a large range of atmospheric $CO_2$ levels and the presence or absence of a gateway between the Pacific and Arctic Oceans. These experiments allow us (1) to improve our understanding of the relative impact of radiative and tectonic forcings on the Maastrichtian climate/ocean system and (2) to assess which set of boundary conditions better matches the observed isotopic pattern and leads to the formation of North Pacific deep water.

## 2. Model Description

[5] The model used in this study has been fully described by *Petoukhov et al.* [2000]. CLIMBER-2 is an Earth Model of Intermediate Complexity (EMIC), positioned between simple models (1- or 2-D) and 3-D climate GCMs [*Claussen et al.*, 2002]. The atmospheric component is a 2.5-dimensional dynamical-statistical model which includes many of the processes that are also described in more sophisticated GCMs. In contrast with GCMs, it has a coarse resolution of 10° in latitude and about 51° in longitude. The large-scale circulation (e.g., jets streams and Hadley circulation) and the main high and low pressure cells are explicitly resolved. The atmospheric circulation as well as energy and water fluxes are computed at 10 pressure levels, while long-wave radiation is calculated using 16 levels. To apply the model to the Cretaceous experiments, this module has been kept as in its present form. The ocean module is based on the equations of *Stocker et al.* [1992] and describes the zonally averaged characteristics for three separate ocean basins (Atlantic, Pacific and Indian for the present-day configuration) with a latitudinal reso-

lution of 2.5°. It has 21 levels in the vertical including an upper mixed layer of 50 m thickness. Temperature, salinity, and vertical and meridional velocity are calculated within each basin. The model includes a thermodynamic sea-ice model predicting the sea-ice fraction and thickness for each grid box. The ocean and atmosphere modules are linked by a coupler which calculates the fluxes of energy, momentum and water between the atmosphere and the ocean. Each atmospheric model grid box consists of one or several of six surface types (open-water, sea-ice, tree, grass, bare soil and glaciers). CLIMBER-2 includes a vegetation model, VECODE [*Brovkin et al.*, 1997, 2002], coupled to the atmospheric model. Soil processes are described within a two-layer soil model.

[6] CLIMBER-2 successfully simulates the main features of the modern climate [*Ganopolski et al.*, 1998; *Petoukhov et al.*, 2000] and compares well with GCM results for the quaternary climate [*Kubatski et al.*, 2000; *Ganopolski et al.*, 2001]. It has been used more recently for the onset of glaciation 115ky BP [*Kageyama et al.*, 2004]. CLIMBER-2 has also been successfully applied to pre-quaternary climates like that of Neoproterozoic [*Donnadieu et al.*, 2004a, 2004b].

## 3. Forcing and Boundary Conditions

[7] Prescribed conditions for the model include land-sea distribution, elevation and bathymetry, routage of runoff, solar luminosity, and atmospheric $CO_2$ levels. The terrestrial vegetation model VECODE was used in its dynamic configuration and therefore interacts with the climate model until equilibrium. For the simulation of the Maastrichtian climate, we used the present-day solar orbital configuration and a solar constant 0.65% less than at present [*Gough*, 1981]. The SST field was initialized using a simple cos function, and the initial SSS field was prescribed as 34.7 ppt at each grid cell.

[8] The Maastrichtian paleogeography has been reconstructed accounting for the paleoposition of continents, the location of the mountain ranges and their respective estimated elevations at that time, as well as the paleoshoreline. The paleopositions of large continents have been calculated using both oceanic kinematic parameters and the more recent apparent polar wander paths (to fix the paleolatitude grid) [*Besse and Courtillot*, 1991, 2002]. The positions of continents do not differ drastically from other reconstructions except for the southeastern Asian margin. As we have no direct evidences for the elevations of mountain ranges in the past, this parameter remains difficult to estimate. To overcome this difficulty, we compared the geodynamic context at that time with present-day analogue in order to attribute an elevation to each grid cell. The only significant mountain reliefs (above 600 m) are located (1) in southern Laurasia (up to about 900 m high) because of the gradual consolidation of many Asian land blocks and (2) along the western coast of North America (up to 1200 m) due to the Sevier orogeny and to the Colorado Laramide orogeny. The shoreline has been mapped according to literature [*Camoin et al.*, 1993; *Philip and Floquet*, 2000; *Scotese*, 2001].

[9] The longitudinal distribution of each basin for the ocean module has been adapted for the Cretaceous (Figure 1). As our study mainly focuses on oceanic circulation changes in the Pacific Ocean, we ensure that the Pacific Ocean, identified as basin 3, is well represented. Basin 2, which represents the Atlantic Ocean, also includes the Mediterranean Tethys and part of the Indian Ocean.

[10] Because river drainage basins are poorly defined for this time period, we defined a river mask in which rain falling and snowmelt on land is equally redistributed to all coastal land points, except on the western North America coast where the runoff is distributed for one half to the west (Pacific) and for the other half to the east (Western Interior Seaway), because of the presence of N-S mountains in this area [*Jordan*, 1981; *Hay et al.*, 1999]. Bathymetry is specified at 5000 m for oceanic basins, at 200 m on platforms and epicontinental seas, and at 2500 m in the Arctic. Geography of the Arctic Ocean and its connections to the World Ocean during the Maastrichtian stage still remain uncertain [*Magavern et al.*, 1996]. During the Jurassic and Early Cretaceous, accretion of island arcs terranes occurred in the NE Siberia-Alaska region, followed by the formation of the Okhotsk-Chukotka volcanic belt during the late Early to Late Cretaceous interval, linked to the northward subduction of the Kula oceanic plate under the newly assembled tectonic collage [*Hourigan and Akinin*, 2004]. This tectonic structure, which separated the Arctic Ocean from the North Pacific, spans a length of ~3000 km for a width of a few hundreds of kilometers [*Miller et al.*, 2002]. As substantial sea level changes have been identified throughout the Maastrichtian [*Miller et al.*, 1999], it is plausible that this volcanic belt and accreted terranes provided a high latitude land

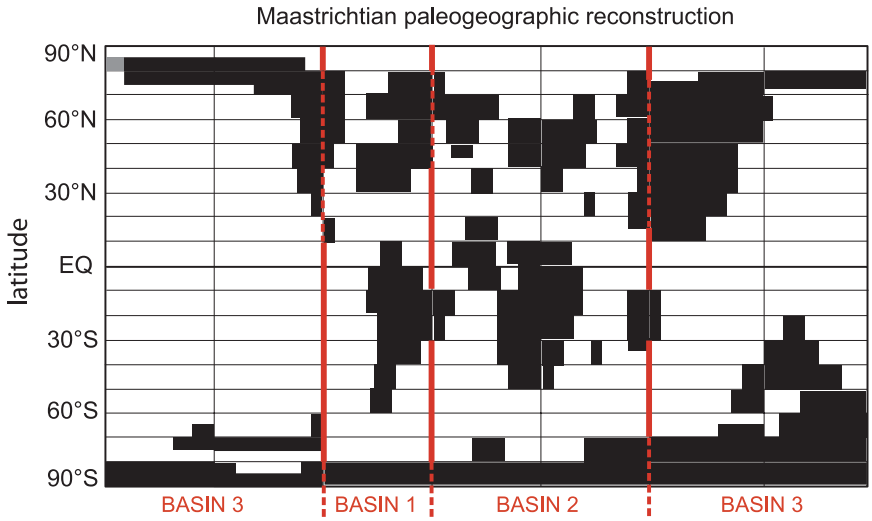


**Figure 1.** Paleogeographic reconstruction for the Maastrichtian with the CLIMBER-2 grid, established using the procedure described by *Besse and Courtillot* [1988]. The gray area represents land for closed marine communications between the Arctic and North Pacific oceans (CASE1) and ocean for opened marine communications between the Arctic and North Pacific oceans (CASE2). The thick red lines show the separations between the three oceanic basins.

bridge between Asia and Alaska during periods of sea level drops and was recovered by a shallow marine passage during periods of higher sea level. Isotopic ($^{87}Sr/^{86}Sr$) as well as paleontologic (based on phytoplankton and sillicoflagellate affinities) evidences support the existence of shallow marine communications between the Arctic and the Pacific during part of the Maastrichtian interval [*Magavern et al.*, 1996]. We therefore examine the sensitivity of the Maastrichtian ocean-climate system taking into consideration uncertainty in the precise paleogeographic reconstruction in this area (see Figure 1). Two sensitivity tests have been conducted: one precluding marine communications between the Arctic and North Pacific oceans (CASE1), and the other allowing a shallow (100 m deep) marine gateway between the two oceans (CASE2). As two layers of 50 m are required in CLIMBER-2 for water exchange between two basins or parts of a basin, it was not possible to test the impact of a shallower gateway on our results. Note, however, that in order to simulate this gateway, only a limited part of the land bridge between Asia and Alaska is covered by 100 m of water in CASE2 experiments (Figure 1).

[11] Reconstructions of atmospheric carbon dioxide ($CO_2$) concentrations for the Maastrichtian encompass a range of <280 ppm to about 1500 ppm volumetrically [*Royer et al.*, 2004]. Both the upper bound (1110–1850 ppm [*Ghosh et al.*, 2001]) and lower bound (0–210 ppm [*Ekart et al.*, 1999]) to this range comes from soil carbonate proxy records. We therefore investigate the response of the Maastrichtian ocean-climate system to atmospheric $CO_2$ forcing for the two different paleogeographies described above, using 7 different $pCO_2$ within the range proposed from proxy records: 280 ppm (1x pre-industrial value), 350 ppm (1.25x), 420 ppm (1.5x), 560 ppm (2x), 840 ppm (3x), 1120 ppm (4x), and 1400 ppm (5x). For each simulation the model is ran until equilibrium (5000 years).

## 4. Results

[12] In agreement with all recent simulations realized for the latest Cretaceous period, none of our simulations show the existence of deep warm and saline waters formed at low latitude [e.g., *Brady et al.*, 1998; *DeConto et al.*, 2000; *Otto-Bliesner et al.*, 2002]. Deep waters always form at high latitudes in our simulations. However, depending on atmospheric $CO_2$ level and on the state (open/closed) of the marine communications between the Arctic and North Pacific, deep water can be produced at different high latitude sites and several modes of thermohaline circulation can be observed in our simulations.

### 4.1. Results for CASE 1

[13] When marine communications between the North Pacific and the Arctic oceans are closed, the North Pacific region is always a site of formation of deep or intermediate water, independently

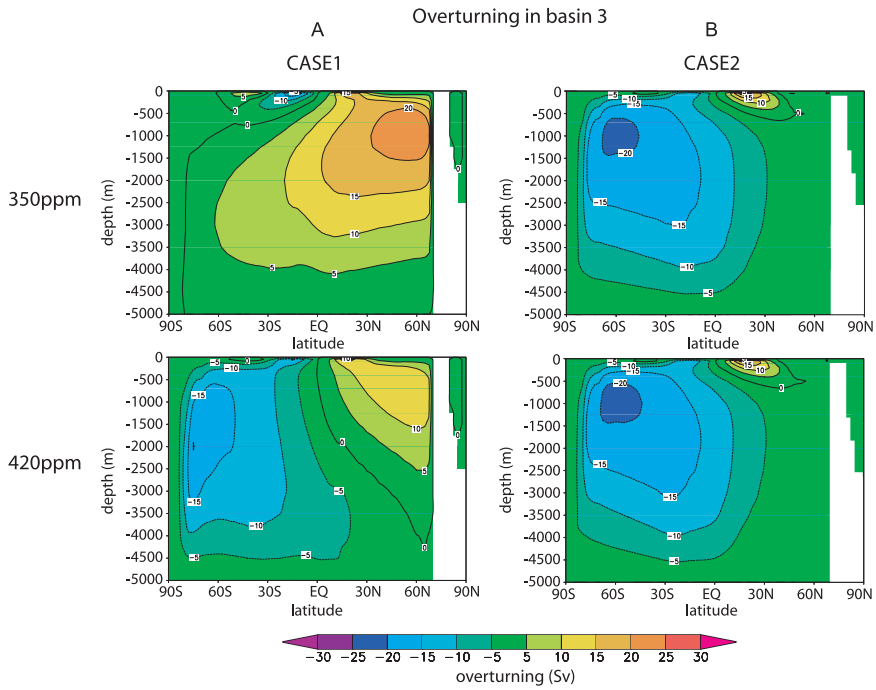


**Figure 2.** Vertical mean annual overturning stream function simulated in the (a) CASE1 and (b) CASE2 runs for basin 3 and for a prescribed atmospheric $CO_2$ of 350 ppm and 420 ppm. Positive overturning represents clockwise transport. Negative contours are dashed.

of $CO_2$ atmospheric level prescribed in the simulation. However, a threshold between two modes of thermohaline circulation is passed between 420 ppm and 350 ppm. For atmospheric $pCO_2$ above 350 ppm, the North Pacific convection cell only reaches about 2500 m, and a deeper convection cell is present in the South Pacific (down to 4500 m; Figure 2a). Therefore, although intermediate waters are still produced in the North Pacific, the main site of deep water production is located in the South Pacific (with maximum overturning of about 15–20 Sv). Between 420 ppm and 1400 ppm, thermohaline circulation changes little, except for a slight decrease in the intensity of the southern hemisphere overturning cell, as a consequence of the overall increase of temperature which lowers the density of the high latitude surface waters.

[14] Below 420 ppm, convection ceases in the South Pacific to be replaced by a strong overturning cell down to 4500 m in the North Pacific (maximum overturning over 25 Sv; Figure 2a). The abrupt switch in thermohaline circulation is a consequence of the readjustment of the sea ice margin latitudinal position related to the atmospheric $CO_2$ level change and consequent temperature decrease. If ice growth during winter induces a temporary salinity increase of the surface waters which can then be able to sink and leave the upper ocean, melting of sea ice during the summer delivers large freshwater fluxes in the front of the ice margin which remain in the upper ocean. The net result of this effect in this region is a decrease of the surface water salinity and therefore of its density. For atmospheric $CO_2$ levels lower than 420 ppm, significant ice melting during summer occurs in the 50–70°S latitude slice (Figure 3), inducing a net salinity decrease of the surface waters in this area which precludes the establishment of a convection cell in the South Pacific. From 350 ppm to 420 ppm, the sea ice margin migrates toward higher latitudes and ice melting during the summer is constricted poleward in the 60–80°S latitude range (Figure 3). The salinity increase around 60°S, which arises from the removal of the melting sea ice component in the freshwater fluxes (Figure 4a), allows a convection cell to develop in the South Pacific. In order to ascertain the significance of the sea ice freshwater-feedback on the overturning, the 350 ppm experiment has been re-run by removing the freshwater component derived from sea ice melting poleward of 40°S (experiment called "CASE1_SIS" as Sea Ice Sensitivity). An overturning cell appears in the South Pacific when this freshwater component is removed poleward of 40°S (the resulting overturning is similar to that shown in Figure 2a for 420 ppm).

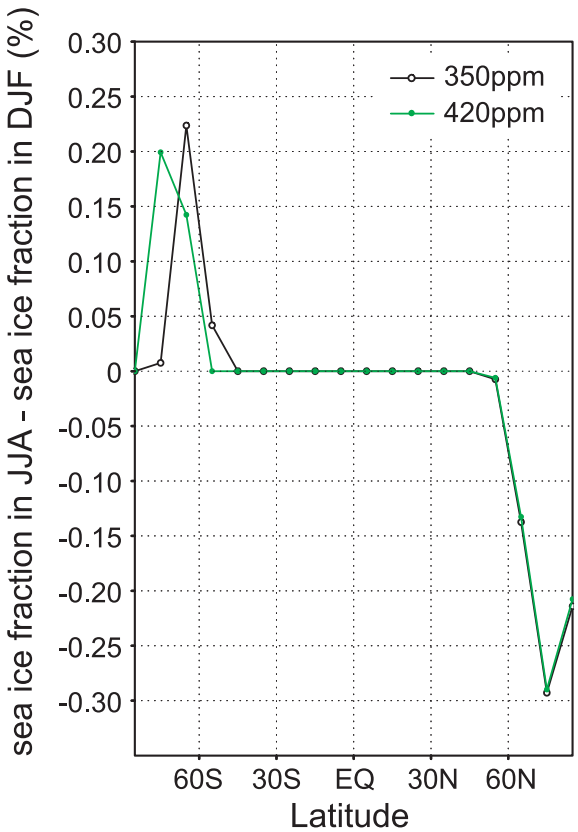


**Figure 3.** Distribution with latitude in basin 3 of annual sea ice melting fraction, represented by the difference of sea ice fraction from June to August (JJA) and sea ice fraction from December to February (DJF), for closed marine communications between Arctic and Pacific (CASE1) and a prescribed atmospheric $CO_2$ of 350 ppm (black open circles) and 460 ppm (green solid circles).

[15] The readjustment of the sea ice margin latitudinal position, which drives the observed thermohaline circulation change between the 350 ppm and 420 ppm experiments, derives from interactions occurring between the atmosphere and the ocean. First, the increase of atmospheric $CO_2$ from 350 ppm to 420 ppm warms the atmosphere and induces the melting of sea ice. The reduction of the sea ice area contributes to decrease the high latitude surface albedo, which amplifies the high latitude warming (Figure 5a) and therefore the sea ice melting (ice albedo feedback). Second, the initiation of convection in the southern region of basin 3, which results in a larger energy transport to the southern high latitudes (Figure 5d), promotes the thermal air surface temperature gradient reduction in the southern hemisphere (Figure 5a). This in turn enhances the melting of sea ice in the southernmost region of basin 3 and therefore contributes to the stability of the new thermohaline mode. The reduction of the surface air temperature gradient then results in a decrease of the wind stress in the southern mid latitudes of basin 3 (Figure 5b). In addition, the E-P increase in the southern region of basin 3 contributes to the stability of new thermohaline circulation equilibrium (Figure 5c).

[16] Regardless of atmospheric $CO_2$ levels, there is no significant overturning in the basin 1 and basin 2, although minor (maximum overturning of 5 Sv) and quite shallow (down to 1000–1500 m depth) convective mixing occurs for $pCO_2$ higher than 350 ppm in the south of both basins (not shown).

[17] Our results for 1120 ppm and for closed marine communications between the Arctic and North Pacific oceans compare well with those found by *Otto-Bliesner et al.* [2002] for the Campanian using 3-D Global Circulation Models with the same atmospheric $CO_2$ level and comparable geography (including closed Pacific-Arctic marine communications). Similarly to the simulation of *Otto-Bliesner et al.* [2002] for 1120 ppm, our results show sinking in high latitude North and South Pacific.

## 4.2. Results for CASE 2

[18] The opening of marine communications between the North Pacific and the Arctic oceans inhibits the formation of deep and intermediate water in the North Pacific region, even in the case of very shallow (100 m deep) communications (Figure 2b). This phenomenon derives from the incursion in the North Pacific of surface waters with marked low salinity from the Arctic Ocean (Figure 4). Due to the consequent salinity decrease in the North Pacific region, the surface waters are not dense enough to sink, regardless of the atmospheric $CO_2$ level and surface water temperature in this region. The atmosphere behavior follows here the oceanic circulation change initiated by the opening of the gateway. The collapse of the northern convection cell in basin 3 results in a slight increase of the northern air surface temperature gradient (Figure 6a), as less heat is brought in the northern high latitudes by the ocean (Figure 6d). However, despite the cooling of the northern high latitude temperatures, which would tend to favor convection through a steeper equator-pole density gradient, convection is still inhibited in this region by the incursion of the low salinity Arctic surface waters. This suggests that in this case the atmosphere follows the ocean and not the opposite although the E-P decrease in the North Pacific

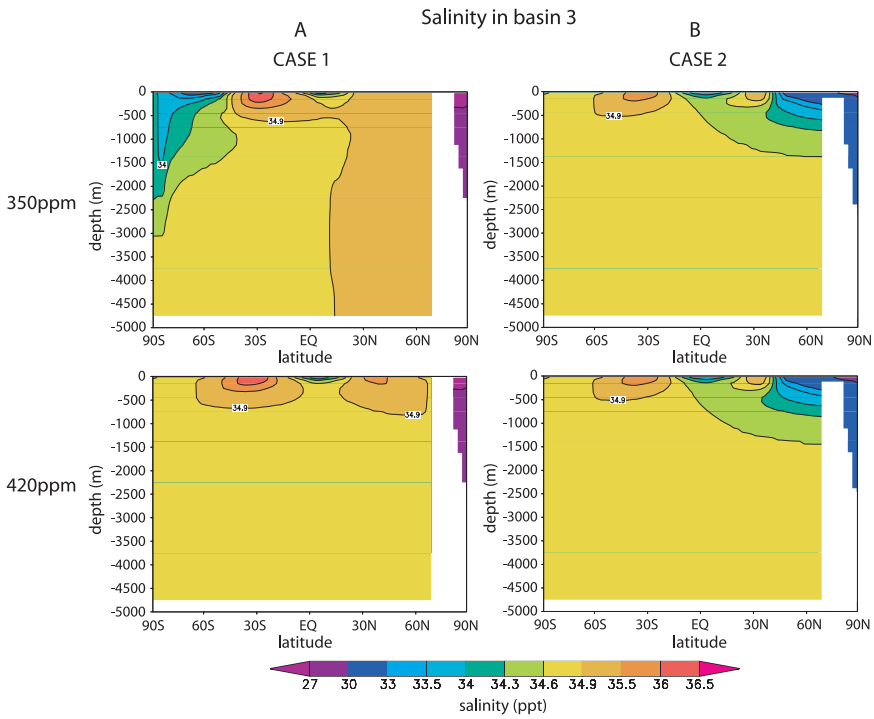


**Figure 4.** Latitude-depth cross section of annual ocean salinity for the basin 3 simulated in the (a) CASE1 and (b) CASE2 runs for prescribed atmospheric $CO_2$ of 350 ppm and 420 ppm. Note the uneven scale used to highlight the changes.

region partly contributes to the stability of new thermohaline circulation equilibrium (Figure 6c). The steeper air surface temperature gradient results in a slightly larger wind stress in the northern region of basin 3 (Figure 6b).

[19] The circulation in the basin 3 is not affected by changes in atmospheric $CO_2$ levels. However, above 420 ppm an overturning cell develops in the southern region of basin 2 with water sinking at high southern latitudes down to 4000 m (maximum overturning of 10–15 Sv; Figure 7). Similarly to basin 3 in CASE1, this is a result of the poleward migration of the ice margin, although occurring here at higher atmospheric $CO_2$ levels, from 420 ppm to 560 ppm. In order to ascertain the significance of the sea ice freshwater-feedback on the overturning, the 420 ppm experiment has been re-run by removing the freshwater component derived from sea ice melting poleward of 40°S. An overturning cell appears in the south of basin 2 when this freshwater component is removed poleward of 40°S (not shown).

## 5. Discussion and Conclusions

[20] Planktic and benthic foraminifera $\delta^{18}O$ records from most of available ODP/DSDP sites show an increase from 75 to 65.5 Ma, indicating that surface and intermediate or deep waters cooled, particularly at high latitudes [*Barrera and Savin*, 1999; *Frank and Arthur*, 1999]. Superimposed on this long-term trend there were two episodes during which, on a global scale, benthic foraminifera $\delta^{18}O$ values increased substantially by 0.5–1.0 permil, and then decreased. The first episode occurred during the Early Maastrichtian (71–69.5 Ma [*Barrera and Savin*, 1999]) and is accompanied by an increase of planktonic foraminiferal $\delta^{18}O$ values indicating that at least in the high southern latitudes surface waters also cooled at about 71 Ma, although the subsequent warming at around 69.5 is less well defined than by the benthic foraminifera [*Barrera et al.*, 1997]. The second, for which the isotopic data set is much smaller, occurred during the Late Maastrichtian (from about 68 Ma to about 65.5 Ma [*Barrera and Savin*, 1999]).

[21] Benthic foraminiferal $\delta^{13}C$ patterns have been used to suggest that during the Early Maastrichtian cool event, deep or intermediate waters formed temporarily in the North Pacific and traveled into the South Pacific and South Atlantic oceans. This is suggested by decreasing $\delta^{13}C$ values of the benthic foraminifera from the equatorial Pacific to the Southern Ocean. After this event, the trend

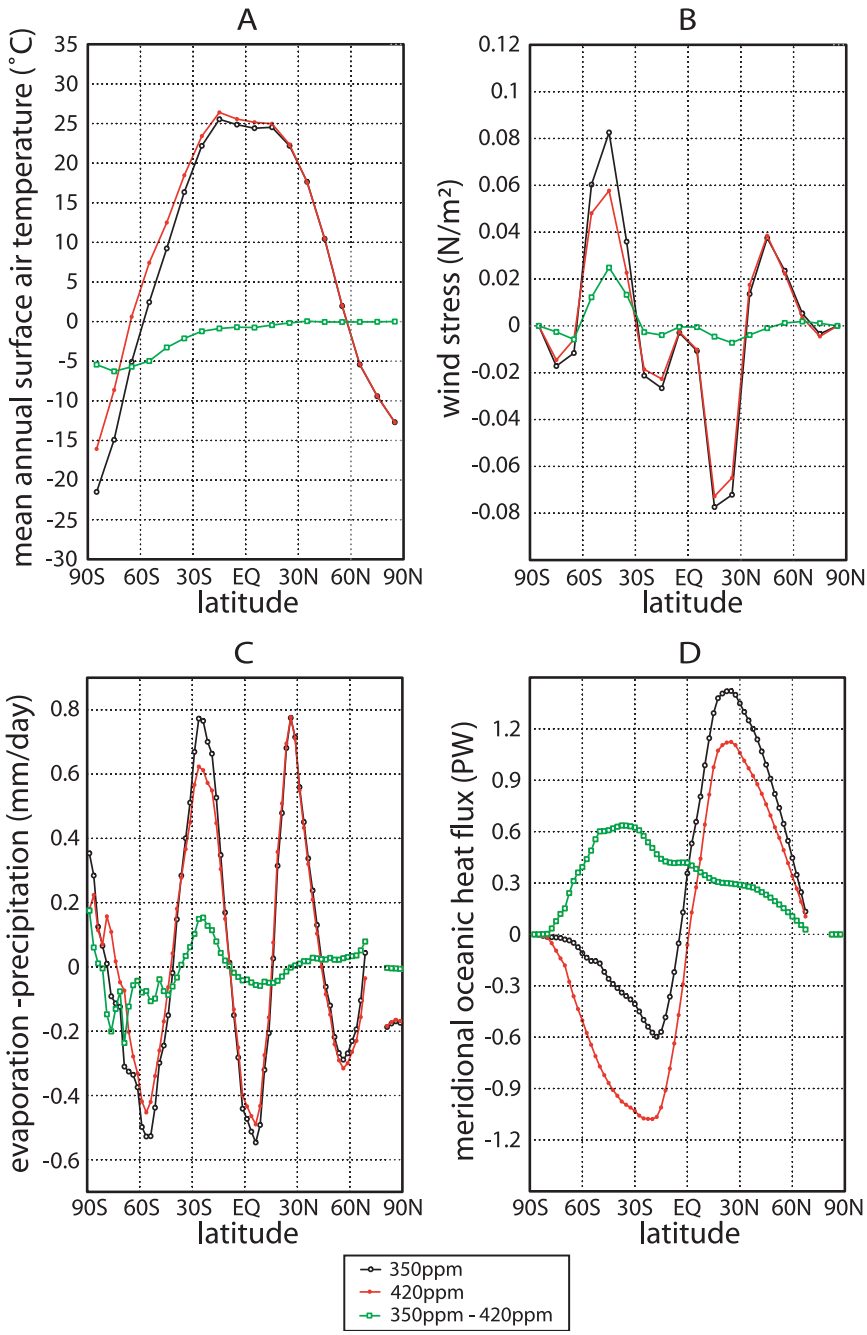


**Figure 5.** Modeled mean annual (a) air surface temperature, (b) wind stress, (c) evaporation-precipitation, and (d) meridional oceanic heat flux, zonally averaged over basin 3 in the 350 ppm (black line and open circles) and 420 ppm (red line and red circles) CASE1 experiments. The green lines represent the difference between the 350 ppm and 420 ppm experiments for each plotted variable.

is reversed, the $\delta^{13}C$ values of benthic foraminifera increasing from the Southern Ocean to the equatorial Pacific, suggesting that deep or intermediate water would have formed in the Southern Ocean and traveled northward as far as the equatorial Pacific [*Barrera et al.*, 1997; *Barrera and Savin*, 1999].

[22] Our results demonstrate that the absence or presence of a marine gateway between the Arctic and North Pacific oceans, along with slight changes in atmospheric $pCO_2$ levels, triggers a shift in the thermohaline circulation mode in agreement with data described above. Furthermore, our simulations suggest that salinity may have been the

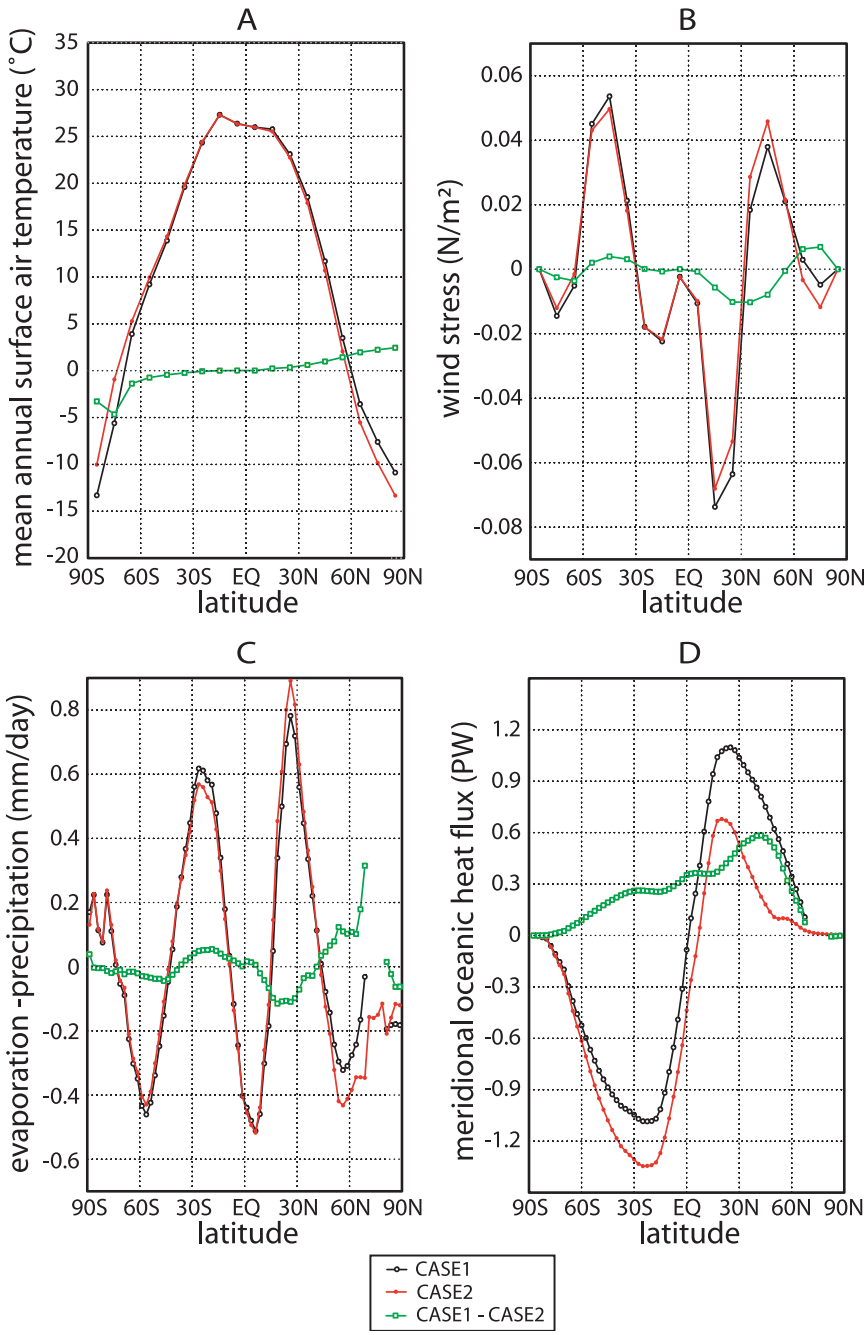


**Figure 6.** Modeled mean annual (a) air surface temperature, (b) wind stress, (c) evaporation-precipitation, and (d) meridional oceanic heat flux, zonally averaged over basin 3 in the CASE1 (black line and open circles) and CASE2 (red line and red circles) experiments for a prescribed $pCO_2$ of 560 ppm. The green lines represent the difference between the CASE1 and CASE2 experiments for each plotted variable.

primary driving factor of the thermohaline circulation during the Maastrichtian period, whereas the influence of surface water temperature distribution appears to be less crucial, except indirectly through the growing or melting of sea ice at high latitude.

[23] The oceanic circulation simulated for CASE1 (closed Arctic-Pacific gateway) and $pCO_2$ lower than 420 ppm reproduces well the thermohaline circulation pattern inferred from benthic foraminiferal $\delta^{13}C$ for the Early Maastrichtian cool event. The main site of deep water production is located in the North Pacific, and intermediate or bottom waters travel southward toward the Southern Ocean (Figure 2a), in agreement with the southward decrease of the benthic foraminifera carbon isotope

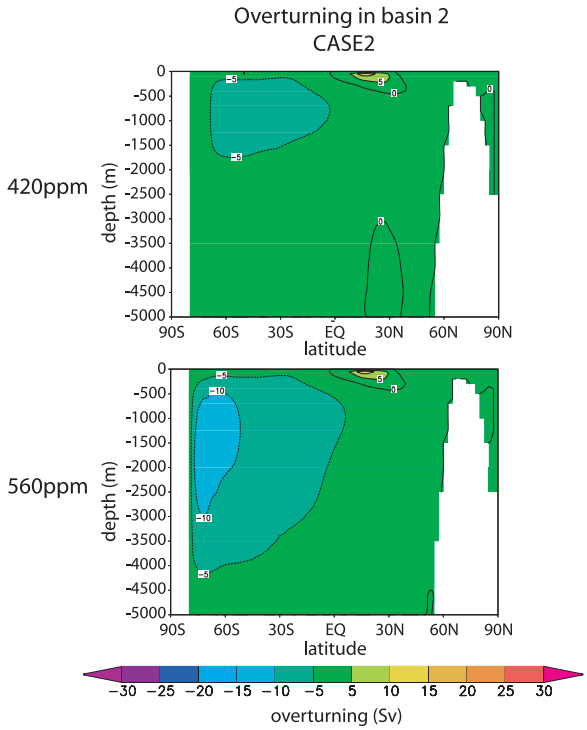


**Figure 7.** Vertical mean annual overturning stream function simulated in the CASE2 runs for basin 2 and for a prescribed atmospheric $CO_2$ of 420 ppm and 560 ppm. Positive overturning represents clockwise transport. Negative contours are dashed.

composition which reflects the aging of the water mass. Simulated intermediate water temperatures in the basin 3 for the run at 350 ppm (3–5°C at about 1500–800 m; Figure 8) are slightly cooler with isotopic temperatures of intermediate waters (800–1500 m) in the Pacific and Indian oceans inferred from the $\delta^{18}O$ of benthic foraminifera, which are typically of 5–7°C in average during the cool Early Maastrichtian event [*Barrera and Savin*, 1999].

[24] The oceanic circulation for CASE2 (opened Arctic-Pacific gateway) and $pCO_2$ higher that 420 ppm compares well with the thermohaline circulation pattern inferred from benthic foraminiferal $\delta^{13}C$ for the Late Maastrichtian. The intermediate or deep water that was produced in the North Pacific for CASE1 is replaced in CASE2 by sinking in the Pacific sector of the Southern Ocean (Figure 2b). For $pCO_2$ above 420 ppm, the southern region of basin 2 provides an additional source of deep waters (Figure 7), which is consistent with the merging of $\delta^{18}O$ values of benthic and planktonic foraminifera at site 690 (70°S, Atlantic Ocean [*Stott and Kennett*, 1990]) suggesting sinking in the South Atlantic during the Late Maastrichtian. The best agreement of the simulated intermediate water temperatures in the basin 3 with isotopic temperatures inferred from the $\delta^{18}O$ of benthic foraminifera (typically of about 7–9°C between 800 and 1500 m [*Barrera and Savin*, 1999]) is obtained with the simulation at 1400 ppm (Figure 7).

[25] However, none of our simulations display sea surface temperatures in the Arctic that match the very warm estimates (about 15°C for the latest Cretaceous) reported by *Jenkyns et al.* [2004] using a new paleothermometer, $TEX_{86}$. Numerical experiments with a prescribed $pCO_2$ higher than 1400 ppm have to be performed to test if such very high Arctic sea surface temperatures can be reproduced by our model.

[26] None of our simulations show deep or intermediate water sinking in the North Atlantic region, in agreement with the results of *Otto-Bliesner et al.* [2002]. This results from the relatively low salinity of the North Atlantic basin (up to several ppt lower than that of the North Pacific at corresponding latitudes; Figure 9a). Because of their low salinity, the North Atlantic surface waters are never dense enough to sink, even at low atmospheric $CO_2$ levels (280 ppm). The low salinity of the Atlantic surface waters derives both from the influence of the quite fresh Arctic Ocean from the north and

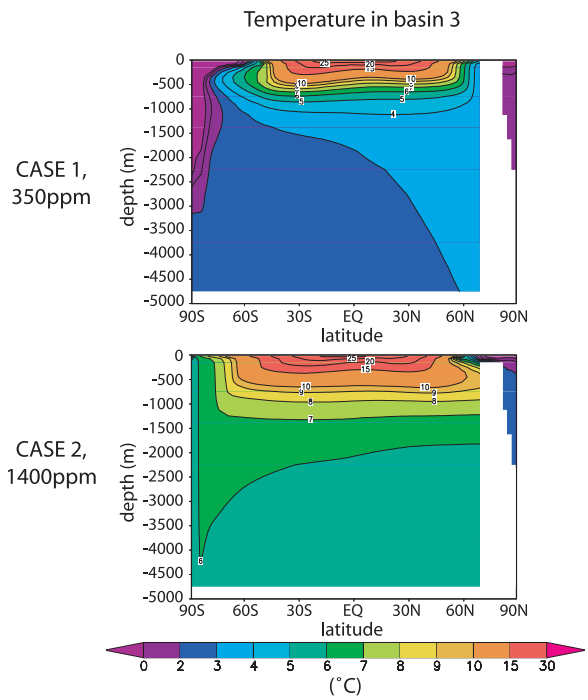


**Figure 8.** Latitude-depth cross section of annual ocean temperature for the basin 3 and for the basin 2 simulated in the CASE1 and CASE2 runs for prescribed atmospheric $CO_2$ of 350 ppm and 1400 ppm, respectively. Line contour interval is 1°C before 10°C and 5°C after.

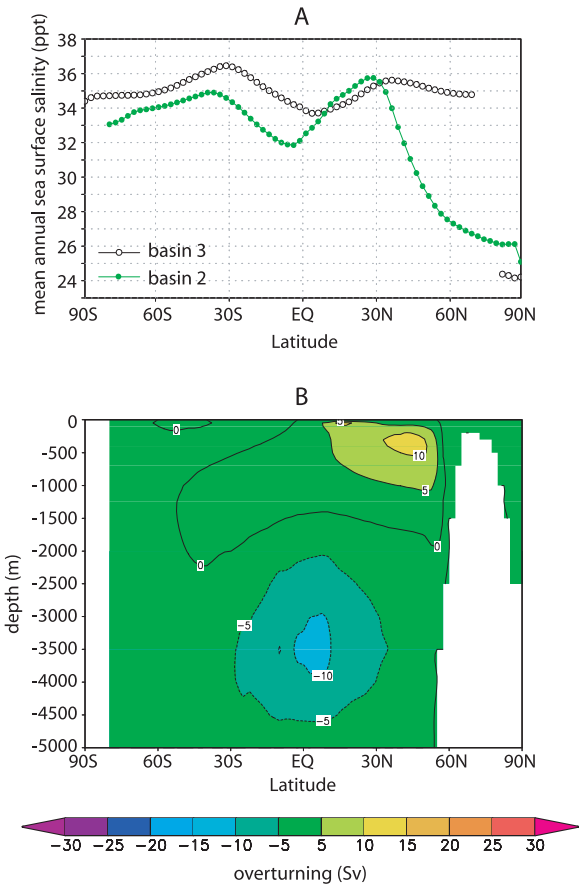


**Figure 9.** (a) Comparison of the mean annual sea surface salinity simulated in the basin 2 (green solid circles) and in the basin 3 (black open circles) in CASE1 runs for a prescribed atmospheric $CO_2$ of 560 ppm. (b) Vertical mean annual overturning stream function simulated in the CASE2_Roff run (runoff removed in basin 2 between 30°N and 60°N) for basin 2 and for a prescribed atmospheric $CO_2$ of 560 ppm. Positive overturning represents clockwise transport. Negative contours are dashed.

from a large runoff between 30 and 60°N which is related to the relative narrowness of the Atlantic Ocean. In order to test the influence of the runoff on the North Atlantic salinity and oceanic circulation, we have realized an additional set of experiments. CASE1 and CASE2 simulations for the seven different $pCO_2$ are repeated with the runoff removed from the North Atlantic between 30°N and 60°N (experiments called "Roff"). Even in this extreme situation, no deep water sinking occurs in the North Atlantic, although an intermediate convection cell develop down to 1000 m deep for CASE2_Roff experiments (maximum overturning of 10 Sv), regardless of the atmospheric $CO_2$ level (Figure 9b). The Arctic influence alone remains sufficient to preclude deep water convection. Therefore our results do not support deep water production in the North Atlantic Ocean during the Maastrichtian period.

[27] *Barrera* [1994] and *Barrera et al.* [1997] demonstrated that the timing of the reversal of the thermohaline circulation during the Early Maastrichtian cool event could be correlated with sea level regression proposed by *Haq et al.* [1987]. *Miller et al.* [1999] inferred the amplitude of this sea level drop to have been of at least 25 m. *Barrera et al.* [1997] and *Barrera and Savin* [1999] proposed that termination of intermediate or deep water formation at low latitudes related to decreasing areas of epicontinental seas during the regression could have caused the reversal in thermohaline circulation during the Early Maastrichtian cool event. Our simulations show no evidence for formation of deep or intermediate waters at low latitudes. Conversely, on the basis of our results, we suggest an alternative mechanism by which a sea level fall could have triggered a change in thermohaline circulation. At about 71–70 Ma, the general regression could have resulted in the closing of marine connections between the North Pacific and Arctic oceans through the emersion of a land bridge formed by the Okhotsk-Chukotka volcanic belt and accreted terranes. As shown with CASE1 simulations, the increased salinity in the North Pacific resulting from the shutdown of the low-salinity Arctic water imports would have allowed intermediate and deep water to form in this area. Southward export of deep and intermediate North Pacific waters as far as the Southern Ocean region is only obtained with a prescribed atmospheric $CO_2$ level of less than 420 ppm.

[28] The subsequent transgression [*Miller et al.*, 1999] would have resulted in the flooding of the land bridge between Asia and Alaska, allowing again shallow marine connections between the Arctic and North Pacific after 69.5 Ma. As the low-salinity Arctic surface waters flowed into the Pacific, leading to a decrease of the North Pacific surface water salinity, the North Pacific waters became not dense enough to sink. The North Pacific deep water source is replaced by sinking in the Pacific sector of the Southern Ocean. Additional sinking in the southern region of basin 2, which produces the best agreement with isotopic patterns, is achieved only for $pCO_2$ above 420 ppm. Increased atmospheric $CO_2$ levels may be promoted by decreasing area of exposed continents during the transgression, through decreased $CO_2$ consumption

by silicate alteration. *Miller et al.* [1999, 2004] have interpreted the Early Maastrichtian sea level drop to be related to the growing of a limited continental ice sheet. The simulations for CASE1 (closed Arctic-Pacific connections) and atmospheric $CO_2$ levels lower than 420 ppm show the presence of perennial ice on continents at high latitude, whereas the simulations for CASE2 (opened Arctic-Pacific connections) and atmospheric $CO_2$ levels of 1400 ppm do not display perennial ice any more (not shown). Our work therefore supports glacio-eustasy as a possible driving mechanism for sea level changes during the Maastrichtian interval.

[29] To summarize, our new set of coupled atmosphere-ocean model simulations with subtle changes in the paleogeography argues for a preponderant role of the Arctic-Pacific gateway during the Maastrichtian period. Our results also suggest that important fluctuations in the atmospheric $CO_2$ level (spanning between 350 and 1400 ppm) are required to match the changes in oceanic circulation and temperatures inferred from the $\delta^{18}O$ and $\delta^{13}C$ of Maastrichtian benthic foraminifera. Such a short-term high variability in the $pCO_2$ has already been suggested by *Bice and Norris* [2002] for the Cretaceous period. Our tentative scenario requires sea level variations which may be interpreted as the consequence of the ice sheet build up during the cool event. While explorative rather than exact, given the intermediate complexity of the model, our contribution raises question for geochemical modelers as one needs to find mechanisms capable of inducing large changes in $CO_2$ content of the Maastrichtian atmosphere. Future modeling effort focused on understanding and quantifying the interplay between sea level drawdown, ice volume and global climate during this peculiar period should reveal useful. The development of a coupling between the CLIMBER-2 model and the 3-D Ice Sheet Model GREMLINS [*Ritz et al.*, 1997; *Kageyama et al.*, 2004] holds great promise in this regard.

## Acknowledgments

[30] We are grateful to two anonymous reviewers who provided very constructive comments that greatly helped to improve this manuscript. The work was funded by the CNRS French program ECLIPSE. We thank the PIC team for providing the CLIMBER-2 model.

## References

Barrera, E. (1994), Global environmental changes preceding the Cretaceous-Tertiary boundary: Early-late Maastrichtian transition, *Geology*, *22*, 877–880.

Barrera, E., and S. M. Savin (1999), Evolution of late Campanian-Maastrichtian marine climates and oceans, in *Evolution of the Cretaceous Ocean-Climate System*, edited by E. Barrera and C. C. Johnson, *Spec. Pap. Geol. Soc. Am.*, *332*, 245–282.

Barrera, E., S. M. Savin, E. Thomas, and C. E. Jones (1997), Evidence for thermohaline-circulation reversals controlled by sea-level change in the latest Cretaceous, *Geology*, *25*, 715–718.

Barron, E. J., P. J. Fawcett, W. H. Peterson, D. Pollard, and S. L. Thompson (1995), A "simulation" of mid-Cretaceous climate, *Paleoceanography*, *10*, 953–962.

Besse, J., and V. Courtillot (1988), Paleogeographic maps of the Indian Ocean bordering continents since the Upper Jurassic, *J. Geophys. Res.*, *93*, 11,791–11,808.

Besse, J., and V. Courtillot (1991), Revised and synthetic apparent polar wander paths of the African, Eurasian, North America and Indian Plates, and true polar wader since 200 Ma, *J. Geophys. Res.*, *96*, 4029–4050.

Besse, J., and V. Courtillot (2002), Apparent and true polar wander and the geometry of the geomagnetic field over the last 200 Myr, *J. Geophys. Res.*, *107*(B11), 2300, doi:10.1029/2000JB000050.

Bice, K. L., and R. D. Norris (2002), Possible atmospheric $CO_2$ extremes of the Middle Cretaceous (late Albian–Turonian), *Paleoceanography*, *17*(4), 1070, doi:10.1029/2002PA000778.

Brady, E. C., R. M. DeConto, and S. L. Thompson (1998), Deep water formation and poleward ocean heat transport in the warm climate extreme of the Cretaceous (80 Ma), *Geophys. Res. Lett.*, *25*, 4205–4208.

Brovkin, V., A. Ganopolski, and Y. Svirezhev (1997), A continuous climate-vegetation classification for use in climate-biosphere studies, *Ecol. Modell.*, *101*, 251–261.

Brovkin, V., J. Bendtsen, M. Claussen, A. Ganopolski, C. Kubatzki, V. Petoukhov, and A. Andreev (2002), Carbon cycle, vegetation, and climate dynamics in the Holocene: Experiments with the CLIMBER-2 model, *Global Biogeochem. Cycles*, *16*(4), 1139, doi:10.1029/2001GB001662.

Bush, A. B. G., and S. G. H. Philander (1997), The late Cretaceous: Simulation with a coupled atmosphere-ocean general circulation model, *Paleoceanography*, *12*, 495–516.

Camoin, G., Y. Bellion, J. Benkheli, J. J. Cornée, J. Dercourt, R. Guiraud, A. Poisson, and B. Vrielynk (1993), Late Maastrichtian (69.5–65 Ma), in *Atlas Tethys Palaeoenvironmental Maps*, edited by J. Dercourt, L. E. Ricou, and B. Vrielynck, pp. 153–178, Gauthier-Villars, Paris.

Claussen, M., et al. (2002), Earth system models of intermediate complexity: Closing the gap in the spectrum of climate system models, *Clim. Dyn.*, *18*, 579–586.

DeConto, R. M., E. C. Brady, J. Bergengren, and W. W. Hay (2000), Late Cretaceous climate, vegetation, and ocean interactions, in *Warm Climate in Earth History*, edited by B. T. Huber, K. G. MacLeod, and S. L. Wing, pp. 241–274, Cambridge Univ. Press, New York.

Donnadieu, Y., Y. Goddéris, G. Ramstein, A. Nedelec, and J. G. Meert (2004a), A "snowball Earth" climate triggered by continental break-up through changes in runoff, *Nature*, *428*, 303–306.

Donnadieu, Y., G. Ramstein, F. Fluteau, D. Roche, and A. Ganopolski (2004b), The impact of atmospheric and oceanic heat transports on sea-ice-albedo instability during the Neoproterozoic, *Clim. Dyn.*, *22*, 293–306.

Ekart, D. D., T. E. Cerling, I. P. Moñtanez, and N. J. Tabor (1999), A 400 million year carbon isotope record of pedogenic carbonate: Implications for paleoatmospheric carbon dioxide, *Am. J. Sci.*, *299*, 805–827.

Frank, T. D., and M. A. Arthur (1999), Tectonic forcings of Maastrichtian ocean-climate evolution, *Paleoceanography*, *14*, 103–117.

Ganopolski, A., S. Rahmstorf, V. Petoukhov, and M. Claussen (1998), Simulation of modern and glacial climates with a coupled model of intermediate complexity, *Nature*, *391*, 351–356.

Ganopolski, A., V. Petoukhov, S. Rahmstorf, V. Brovkin, M. Claussen, A. Eliseev, and C. Kubatzki (2001), CLIMBER-2: A climate system model of intermediate complexity. Part II: Model sensitivity, *Clim. Dyn.*, *17*, 735–751.

Ghosh, P., P. Ghosh, and S. K. Bhattacharya (2001), $CO_2$ levels in the Late Paleozoic and Mesozoic atmosphere from soil carbonate and organic matter, Satpura basin, Central India, *Palaeogeogr. Palaeoclimatol. Palaeoecol.*, *170*, 219–236.

Gough, D. O. (1981), Solar interior structure and luminosity variations, *Sol. Phys.*, *74*, 21–34.

Haq, B. U., J. Hardenbol, and P. R. Vail (1987), Chronology of fluctuating sea levels since the Triassic (250 million years ago to present), *Science*, *235*, 1156–1167.

Hay, W. H., et al. (1999), Alternative global Cretaceous paleogeography, in *Evolution of the Cretaceous Ocean-Climate System*, edited by E. Barrera and C. C. Johnson, *Spec. Pap. Geol. Soc. Am.*, *332*, 1–47.

Hourigan, J. K., and V. V. Akinin (2004), Tectonic and chronostratigraphic implications of new $^{40}Ar/^{39}Ar$ geochronology and geochemistry of the Arman and Maltan-ola volcanic fields, Okhotsk-Chukotka volcanic belt, northeastern Russia, *Geol. Soc. Am. Bull.*, *116*, 637–654.

Jenkyns, H. C., A. Forster, S. Schouten, and J. S. Damsté (2004), High temperatures in the Late Cretaceous Arctic Ocean, *Nature*, *432*, 888–892.

Jordan, T. E. (1981), Thrust loads and foreland basin evolution, Cretaceous western United Stades, *AAPG Bull.*, *64*, 2506–2520.

Kageyama, M., S. Charbit, C. Ritz, M. Khodri, and G. Ramstein (2004), Quantifying ice-sheet feedbacks during the last glacial inception, *Geophys. Res. Lett.*, *31*, L24203, doi:10.1029/2004GL021339.

Kubatski, C., M. Montoya, S. Rahmstorf, A. Ganopolski, and M. Claussen (2000), Comparison of the last interglacial climate simulated by a coupled global model of intermediate complexity and an AOGCM, *Clim. Dyn.*, *16*, 799–814.

Li, L., and G. Keller (1998), Abrupt deep-sea warming at the end of the Cretaceous, *Geology*, *26*, 995–998.

MacLeod, K. G., and B. T. Huber (1996), Reorganization of deep ocean circulation accompanying a Late Cretaceous extinction event, *Nature*, *380*, 422–425.

Magavern, S., D. L. Clark, and S. L. Clark (1996), $^{87}Sr/^{86}Sr$, phytoplankton, and the nature of the Late Cretaceous and Early Cenozoic Arctic Ocean, *Mar. Geol.*, *133*, 183–192.

Miller, E. L., M. Gelman, L. Parfenov, and J. Hourigan (2002), Tectonic setting of Mesozoic magmatism: A comparison between northeastern Russia and the North American cordillera, in *Tectonic Evolution of the Bering Shelf-Chukoki-Sea-Arctic Margin and Adjacent Land Masses*, edited by E. L. Miller, A. Grantz, and S. L. Kemplerer, *Spec. Pap. Geol. Soc. Am.*, *360*, 313–332.

Miller, K. G., E. Barrera, R. K. Olsson, P. J. Sugarman, and S. M. Savin (1999), Does ice drive early Maastrichtian eustasy? Global $\delta^{18}O$ and New Jersey sequences, *Geology*, *27*, 783–786.

Miller, K. G., P. J. Sugarman, J. V. Browning, M. A. Kominz, R. K. Olsso, M. D. Feigenson, and J. C. Hernandez (2004), Upper Cretaceous sequences and sea-level history, New Jersey Coastal Plain, *Geol. Soc. Am. Bull.*, *116*, 368–393.

Otto-Bliesner, B. L., E. C. Brady, and C. Shields (2002), Late Cretaceous ocean: Coupled simulations with the National Center for Atmospheric Research Climate System Model, *J. Geophys. Res.*, *107*(D2), 4019, doi:10.1029/2001JD000821.

Petoukhov, V., A. Ganopolski, M. Claussen, A. Eliseev, C. Kubatzki, and S. Rahmstorf (2000), CLIMBER-2: A climate system model of intermediate complexity. Part I: Model description and performance for present climate, *Clim. Dyn.*, *16*, 1–17.

Philip, J., and M. Floquet (2000), Late Maastrichtian (69.5–65 Ma), in *Atlas Peri-Tethys, Palaeogeographical Maps*, *Map 16*, edited by J. Dercourt et al., CCGM/CGMW, Paris.

Poulsen, C. J., E. J. Barron, C. Johnson, and P. Fawcett (1999), Links between major climatic factors and regional oceanic circulation in the mid-Cretaceous, in *Evolution of the Cretaceous Ocean-Climate System*, edited by E. Barrera and C. C. Johnson, *Spec. Pap. Geol. Soc. Am.*, *332*, 73–90.

Poulsen, C. J., A. S. Gendaszek, and R. L. Jacob (2003), Did the rifting of the Atlantic Ocean cause the Cretaceous thermal maximum?, *Geology*, *31*, 115–118.

Ritz, C., A. Fabre, and A. Letréguilly (1997), Sensitivity of a Greenland ice sheet model to ice flow and ablation parameters: Consequences for the evolution through the last climatic cycle, *Clim. Dyn.*, *13*, 11–24.

Royer, D. L., R. A. Berner, I. P. Montanez, N. J. Tabor, and D. J. Beerling (2004), $CO_2$ as a primary driver of Phanerozoic climate, *GSA Today*, *14*, 4–10.

Scotese, C. R. (2001), Atlas of Earth History, 52 pp., PALEOMAP Proj., Arlington, Tex.

Stocker, T. F., D. G. Wright, and L. A. Mysak (1992), A zonally averaged, coupled ocean-atmosphere model for paleoclimate studies, *J. Clim.*, *5*, 774–797.

Stott, L. D., and J. P. Kennett (1990), The paleoceanographic and paleoclimatic signature of the Cretaceous/Paleogene boundary in the Antarctic: Stable isotope results from ODP leg 113, *Ocean Drill. Program Sci. Results*, *113*, 829–848.